



**HAL**  
open science

## Interpretation of Hopping Transport Based on Pentacene Thin-Film Transistors

Peng Zhang, Emmanuel Jacques, Régis Rogel, Laurent Pichon, Olivier  
Bonnaud

► **To cite this version:**

Peng Zhang, Emmanuel Jacques, Régis Rogel, Laurent Pichon, Olivier Bonnaud. Interpretation of Hopping Transport Based on Pentacene Thin-Film Transistors. IEEE Transactions on Electron Devices, 2023, 70 (12), pp.6364-6368. 10.1109/TED.2023.3326785 . hal-04289629

**HAL Id: hal-04289629**

**<https://hal.science/hal-04289629>**

Submitted on 8 Jan 2024

**HAL** is a multi-disciplinary open access archive for the deposit and dissemination of scientific research documents, whether they are published or not. The documents may come from teaching and research institutions in France or abroad, or from public or private research centers.

L'archive ouverte pluridisciplinaire **HAL**, est destinée au dépôt et à la diffusion de documents scientifiques de niveau recherche, publiés ou non, émanant des établissements d'enseignement et de recherche français ou étrangers, des laboratoires publics ou privés.



Distributed under a Creative Commons Attribution - NonCommercial 4.0 International License

# Interpretation of Hopping Transport Based on Pentacene Thin-Film Transistors

Peng Zhang<sup>1</sup>, Emmanuel Jacques<sup>2</sup>, Régis Rogel, Laurent Pichon<sup>2</sup>, and Olivier Bonnaud

**Abstract**—Organic thin-film transistors (OTFTs) with pentacene active layer were fabricated and analyzed. The electrical parameters were deduced, with the adjusted threshold voltage by modified Y-function method. The derivative field effect mobility was adopted to extract the mobility enhancement factor, which is consistent with the characteristic temperature deduced from density of states (DOS) calculation. The electrical properties of pentacene thin-film transistors were modeled based on variable range hopping (VRH) mechanism, and active layer morphologies were also provided to verify the transport mechanism.

**Index Terms**—Characteristic modeling, density of states (DOS), organic thin-film transistor (OTFT), variable range hopping (VRH) transport.

## I. INTRODUCTION

BEING an important branch of electronics and optoelectronics, organic thin-film transistors (OTFTs) have been proposed in the second mid of the 20th century. Since the 1980s, OTFT technology has undergone several developments thanks to the advantages it offers in terms of lightweight, low-temperature processing that enables flexible applications, environment-friendly, and rich in variety [1], [2], [3]. However, the main shortcoming lies in their relatively low-field effect mobility, which limits their potential applications, especially for providing high current that drives organic light-emitting diodes (OLEDs) in AMOLED displays. Nevertheless, much effort has been made to pursue higher driving capability of OTFTs [4], [5], [6].

One key improvement of the electrical properties is the well understanding of the connection of the electrical characteristics to the carrier transport mechanism. In addition to make progress in improving field effect mobility of OTFTs,

Manuscript received 21 July 2023; revised 3 September 2023 and 2 October 2023; accepted 16 October 2023. This work was supported in part by the Natural Science Foundation of Jiangsu Province under Grant BK20180762 and in part by NUPTSF under Grant NY219099. The review of this article was arranged by Editor X. Guo. (Corresponding author: Peng Zhang.)

Peng Zhang is with the College of Integrated Circuit Science and Engineering, Nanjing University of Posts and Telecommunications, Nanjing 210023, China (e-mail: zp@njupt.edu.cn).

Emmanuel Jacques, Régis Rogel, Laurent Pichon, and Olivier Bonnaud are with the Département OASiS (Organic and Silicon Systems), Institut d'Electronique et des Technologies du numérique, Université de Rennes 1, 35042 Rennes, France (e-mail: emmanuel.jacques@univ-rennes1.fr; regis.rogel@univ-rennes1.fr; laurent.pichon@univ-rennes1.fr; olivier.bonnaud@univ-rennes.fr).

Color versions of one or more figures in this article are available at <https://doi.org/10.1109/TED.2023.3326785>.

Digital Object Identifier 10.1109/TED.2023.3326785

the carrier transport mechanism of OTFTs should also be inspected. In this work based on the relationship between mobility enhancement factor and the characteristic temperature of density of states (DOS), the variable range hopping (VRH) transport mechanism can be verified. The electrical characteristics were also analyzed by relating with morphology observation of pentacene active layer, since energy/space disorder can affect carrier transport.

## II. FABRICATION PROCESS

The fabrication process of bottom-gate, top-contact OTFTs was carried out on silicon substrates. Initially, the 6-in silicon substrate was cut into  $1.5 \times 1.5$  cm slices, the silicon substrate is n-type heavily doped monocrystalline silicon covered with a 300-nm dry-oxidized silicon oxide, which act as the gate electrode and the gate dielectric materials, respectively. The substrates were cleaned with acetone, alcohol, and deionized water, respectively for 10 min, assisted by ultrasound. After drying in the heating oven at 120°C for more than 30 min, a thin polystyrene (PS) layer was spin-coated on the substrates at 3000 r/min for 30 s from a 4-mg/mL solution dissolved in toluene, which is assumed to be able to passivate active layer interface and thus improve active layer morphology. After spinning-coating of PS layer, the samples were annealed at 90°C for more than 30 min. Afterward, pentacene active layers were deposited. The active layer of device A is deposited at low vacuum degree with the chamber pressure of more than  $2 \times 10^{-4}$  Pa, while the active layer of device B is deposited at high vacuum degree with the chamber pressure of approximately  $10^{-4}$  Pa. Higher vacuum is assumed to be better for active layer deposition, especially for elimination of Volmer–Weber grown island-like grains. Finally, a thick copper layer is deposited and patterned by shadow masks to form source and drain contact pads, which defines a channel width/length ratio of 1500/100  $\mu\text{m}$ . Bottom-gate, top-contact OTFT configuration is demonstrated as Fig. 1(a), where pentacene morphology can be controlled by PS passivation layer and by thermal evaporation parameters during pentacene evaporation, such as vacuum level, evaporation rate, and substrate temperature. All the electrical characterizations were carried out by a Keithley 4200 SCS semiconductor parameter analyzer in ambient air.

## III. RESULTS AND DISCUSSION

The typical output characteristics of OTFT are shown in Fig. 1(b). Linear and saturation region are well discriminated

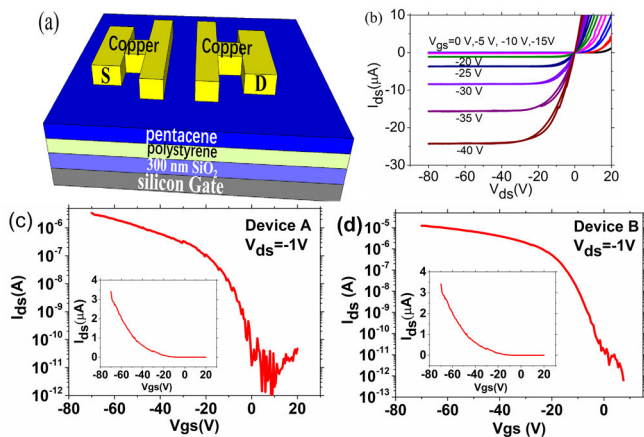


Fig. 1. (a) Bottom-gate, top-contact configuration of OTFT. (b) Output characteristics of typical OTFT. Transfer characteristics of (c) device A and (d) device B.

TABLE I

ELECTRICAL PARAMETERS FOR OTFTS						
	$I_{on}/I_{off}$	$\mu_{FE}$ ( $cm^2/V\cdot s$ )	Conven- tional $V_{th}$ (V)	$V_{th}$ (V) by Y-function method	SS (V/dec)	$\gamma$
A	$1.9 \times 10^5$	0.52	-36.3	-15	4.03	1.73
B	$3.6 \times 10^5$	1.62	-26	-16.8	3.64	3.3

by pinch-off point, indicating the field effect of the OTFT. Hysteresis is not observed with PS passivation layer. For devices A and B, transfer characteristics are demonstrated as Fig. 1(c) and (d), respectively. The drain–source voltage  $V_{ds}$  is set to be  $-1$  V, while the gate–source voltage  $V_{gs}$  ranges from 20 to  $-70$  V. Therefore, the OTFTs work in linear regime, and the electrical parameters can be deduced from the following formula:

$$I_{ds} = \frac{W}{L} C_{ox} \mu_{FE} \left( V_{gs} - V_{th} - \frac{1}{2} V_{ds} \right) V_{ds} \quad (1)$$

where  $W/L$  is channel width/length ratio,  $C_{ox}$  is gate dielectric capacitance per unit area,  $\mu_{FE}$  is effective mobility, and  $V_{th}$  is conventional threshold voltage. The electric parameters for devices A and B are listed in Table I. Both devices A and B show the same order of  $10^5$  for ON/OFF current ratio, while device B shows higher effective mobility. Note that, for device B, mobility degradation is observed at higher gate bias, which limits the ON-current. In addition, when the evaporation is carried out at the vacuum degree of below  $5 \times 10^{-4}$  Pa, the degradation/oxidation of the device is assumed to be negligible, thus the degradation/oxidation at high vacuum degree of  $2 \times 10^{-4}$  Pa or  $10^{-4}$  Pa can be excluded. According to the relation between mobility and gate bias, when the gate bias (electric field) is high, the carriers in the channel are closer to the channel/gate dielectric interface, therefore, the carriers scattering is more serious, which may severely degrade the field effect mobility. The mobility degradation can be eliminated by further improving the gate dielectric layers quality. In addition, for device A, a high conventional threshold voltage of approximately  $-36.3$  V may be inaccurate and needs calibration, and the conventional threshold voltage of device B is approximately  $-26$  V, which will also be calibrated.

TABLE II  
ELECTRICAL PARAMETERS COMPARISON FOR PENTACENE OTFT  
WITH POLYMER GATE DIELECTRICS

Ref.	Conditions	$I_{off}$ (A)	$I_{on}$ (A)	$V_{th}$ (V)	$\mu_{FE}$ ( $cm^2/V\cdot s$ )
[15]	Cross-linked TPGDA, BGTC, vacuum, $V_{DS}=-30V$	$10^{-11}$	$3 \times 10^{-6}$	-18	NA
[16]	CYTOP, BGBC, Ag-PEDOT:PSS, in $N_2$	$10^{-13}$	$10^{-6}$	-3	0.19
[17]	PS, BGTC, ambient	NA	NA	-55	0.06
[18]	$SiO_2$ +Parylene C, BGTC	NA	NA	NA	0.15
[19]	PDMS+OTS, BGTC, $V_{DS}=-60V$	$2.5 \times 10^{-9}$	$3 \times 10^{-5}$	12	0.65
[20]	Cross-linked PVP+OTS, BGTC, ambient, $V_{DS}=-30V$	$2 \times 10^{-10}$	$2 \times 10^{-5}$	-12	0.48
this work	$SiO_2$ +PS, BGTC, ambient, $V_{DS}=-1V$	$3.4 \times 10^{-11}$	$1.2 \times 10^{-5}$	-16.8	1.62

For being more accurate, the threshold voltage can be calibrated from the following formula of modified Y-function method [7]:

$$\frac{I_{ds}}{g_m^{1/2}} = s^{-1/2} (V_{gs} - V_{th})^{1+\gamma'/2} \quad (2)$$

$\gamma'$  is the mobility enhancement factor when considering the relationship of field effect mobility with  $V_{gs}-V_{th}$ , which are deduced to be 1.08 and 0.37 for devices A and B, respectively. Therefore, the calibrated threshold voltages are  $-15$  and  $-16.8$  V, respectively, for devices A and B, as shown in Fig. 2(a) and (b). From the modified Y-function method, both devices A and B show threshold voltage of approximately  $-16$  V, indicating a higher accuracy by the determination of the threshold voltages.

For VRH transport, the field effect mobility is enhanced with gate bias, according to the following formula [8]:

$$\mu = \mu_0 |V_{gs} - V_{FB}|^\gamma \quad (3)$$

where  $\mu_0$  is low-field mobility,  $\gamma$  is mobility enhancement factor, and  $V_{FB}$  is flat-band voltage. The mobility enhancement factor corresponding to flat-band voltage can be obtained from Fig. 3(a) and (b) for devices A and B, respectively. For device A, the mobility enhancement factor is approximately 1.73, while for device B, the mobility enhancement factor is 3.3. The higher mobility enhancement factor for device B may indicate lower energy/space disorder for hopping transport. Note that, in Fig. 3(b), the mobility degradation at higher gate bias is observed.

For VRH transport, the transport is closely related to the density of localized states. The hopping can be from one site to another site that is far away with a lower activation energy,

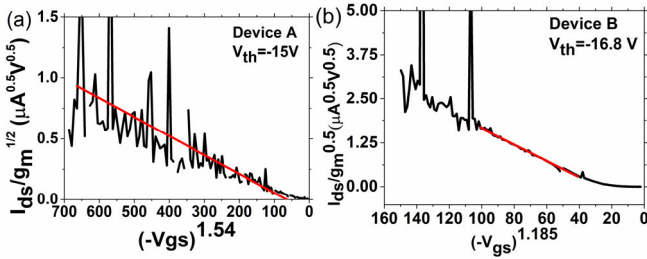


Fig. 2. Threshold voltage extraction of (a) device A and (b) device B from modified Y-function method.

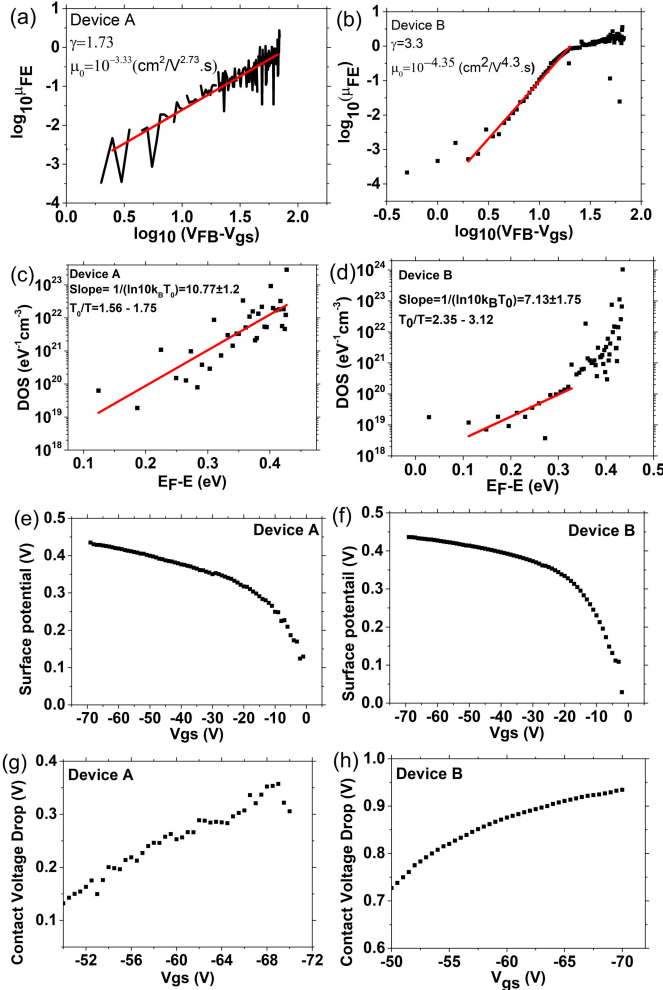


Fig. 3. Mobility enhancement relationship between mobility and gate bias for (a) device A and (b) device B. DOS calculation for (c) device A and (d) device B. Surface potential versus gate bias for (e) device A and (f) device B. Contact voltage drop of (g) device A and (h) device B.

or can be from one site to another close site with a higher activation energy. With the gate bias, the accumulated carriers fill the low-lying energy states, and thus, the activation energy can be reduced with a higher gate bias. Therefore, the mobility enhancement with the gate bias can be observed, while the DOS is critical for analyzing the VRH transport mechanism.

The exponential DOS can be expressed as follows:

$$\text{DOS} = \frac{N_t}{k_B T_0} \exp\left(\frac{-E}{k_B T_0}\right) \quad (4)$$

where  $N_t$  is the number of states per unit volume,  $k_B$  is Boltzmann's constant,  $T_0$  is the characteristic temperature of

exponential DOS, and  $E$  is energy difference. As shown in Fig. 3(c) and (d), the exponential DOS is calculated by Suzuki method [9] for devices A and B, respectively. For the Suzuki method in Fig. 3(c) and (d), the method is based on the amorphous semiconductor TFT, where the DOS calculation is based on the Poisson's equation and Gauss's law, and the band bending calculation is based on field effect, the surface potential is shown as Fig. 3(e) and (f) for devices A and B, respectively. The adopted formulas of Suzuki method are as follows:

$$N_{\text{DOS}}(E_F + q\psi_s) = \frac{\epsilon_{\text{Si}}}{2q^2} \frac{\partial^2}{\partial \Psi_s^2} \left[ \frac{d\Psi(x)}{dx} \Big|_{x=0} \right]^2 \quad (5)$$

$$\frac{d\Psi(x)}{dx} \Big|_{x=0} = -\frac{\epsilon_{\text{Ox}}}{\epsilon_{\text{Si}}} \frac{V_{\text{GS}} - V_{\text{FB}} - \psi_s}{d_{\text{Ox}}} \quad (6)$$

$$d\psi_s = \frac{dG}{G_0} \frac{\epsilon_{\text{Ox}}}{\epsilon_{\text{Si}}} \frac{d}{d_{\text{Ox}}} \frac{V_{\text{GS}} - V_{\text{FB}} - \psi_s}{\exp\left(\frac{q\psi_s}{kT}\right) - 1} \quad (7)$$

where  $\Psi_s$  is the band bending value.

Normally, the molecular density of pentacene is in the order of  $10^{22} \text{ eV}^{-1} \text{ cm}^{-3}$ . In fact, for the DOS calculation in Fig. 3(c), the DOS is mainly smaller than  $10^{22} \text{ eV}^{-1} \text{ cm}^{-3}$ , and the DOS exceeding  $10^{23} \text{ eV}^{-1} \text{ cm}^{-3}$  is due to the instability of the electrical characteristics, which is mainly reflected by the fluctuation of electrical parameters with gate bias, such as the field effect mobility, shown in Fig. 3(a). In contrast, for the DOS calculation in Fig. 3(d), the DOS exceeding  $10^{23} \text{ eV}^{-1} \text{ cm}^{-3}$  is mainly due to the mobility degradation at higher gate bias, as shown in Fig. 3(b).

The contact resistance may limit the electrical characteristics. In order to show the contact resistance, the contact voltage drop can be deduced [10]

$$V_c = (V_{\text{gs}} - V_{\text{th}}) - \sqrt{(2+\gamma)} \left( V_{\text{gs}} - V_{\text{th}} - V_{\text{ds}} \right)^{(2+\gamma)} + I_{\text{ds}} \frac{2 + \gamma}{\mu_0 C_{\text{ox}}} \frac{L}{W}. \quad (8)$$

The extracted contact voltage drop for devices A and B are shown in Fig. 3(g) and (h). For device A, the contact voltage drop is about 0.3 V at  $V_{\text{gs}} = -70$  V, which is small relative to the drain-source voltage  $V_{\text{ds}}$  of  $-1$  V, indicating that the contact resistance is negligible. In contrast, for device B, the contact voltage drop is about 0.92 V at  $V_{\text{gs}} = -70$  V, which is relatively large in comparison to the drain-source voltage  $V_{\text{ds}}$  of  $-1$  V. However, this contact voltage drop should be accurately improved due to that the contact voltage drop calculation corresponds to the degraded mobility of device B, and the cause of mobility degradation is not assured. Further verification work can be carried out, for example, using transmission line method with different channel lengths.

For VRH transport mechanism in OTFTs, the relationship between characteristic temperature and mobility enhancement factor can be expressed as follows [8]:

$$\gamma \approx 2 \frac{T_0}{T} - 2. \quad (9)$$

In Fig. 3(c), as  $\gamma$  is in the range between 1.12 and 1.46, and characteristic temperature  $T_0$  is determined from  $\gamma$ ,  $T_0$  is calculated to be approximately from 468 to 525 K, which

is close to the value of 559.5 K calculated from the mobility enhancement factor. In contrast, for device B, the characteristic temperature  $T_0$  is from 705 to 936 K, which is approximately the value of 795 K calculated from the mobility enhancement factor. In fact, from the original data of transfer characteristics, the DOS accuracy can be ameliorated. Nevertheless, for devices A and B, the primary relationship between characteristic temperature of DOS and mobility enhancement factor can verify the VRH transport mechanism. Note that, the oxygen may introduce deep trap states, as illustrated in [11]. In [11], oxygen and deep trap states are introduced by exposure to oxygen atmosphere for certain time. In contrast, for our case, the measurement is carried out as grown, which eliminates the introduction of oxygen in short time. In addition, due to the top-contact bottom-gate configuration, the gate dielectric/channel interface is at the bottom, and the top layer of pentacene self-encapsulates the channel layer, which also prohibits the intrusion of oxygen in the channel. Therefore, in this measurement, the introduction of deep trap states by oxygen is not considered.

By comparing devices A and B, the high DOS of device A indicates more localized states in the band tail, therefore, device A should have a lower field effect mobility. Indeed, the lower mobility enhancement factor  $\gamma$  of device A in Fig. 3(a) in comparison to Fig. 3(b) verified the low-field effect mobility of device A. However, at higher electric field, mobility degradation of device B increases the DOS, nevertheless, the device B still shows higher field effect mobility at higher electric field.

For VRH transport, the transfer characteristics can be fit by the following formula [12]:

$$I_{ds} = -\beta(V_{FB} - V_{gs})^{\frac{2T_0}{T}} (V_{FB} - V_{GS} \leq |V_{ds}|) \quad (10)$$

$$I_{ds} = -\beta \left[ (V_{FB} - V_{gs})^{\frac{2T_0}{T}} - (V_{FB} - V_{gs} + V_{ds})^{\frac{2T_0}{T}} \right] \times (V_{FB} - V_{GS} > |V_{ds}|) \quad (11)$$

and

$$\mu_0 = \frac{2L}{WC_{ox}} \left( \frac{T_0}{T} \right)^2 \beta. \quad (12)$$

For device A,  $\mu_0 = 10^{-3.33} \text{ cm}^2/(\text{V}^{2.73} \cdot \text{s})$ , therefore,  $\beta = 1.16 \times 10^{-11} \text{ A/V}^{3.73}$ . In contrast, for device B,  $\mu_0 = 10^{-4.35} \text{ cm}^2/(\text{V}^{4.3} \cdot \text{s})$ , therefore,  $\beta = 5.486 \times 10^{-13} \text{ A/V}^{5.3}$ . The modeling of hopping transport for devices A and B can be demonstrated as Fig. 4(a) and (b), respectively, which show the comparison of experimental transfer characteristics and the modeled characteristics. For device A, the experimental and modeled curves fit very well in subthreshold region and ON-state region. For device B, the experimental and modeled curves fit well in subthreshold region and partial ON-state region that  $V_{gs}$  not exceeds approximately  $-25 \text{ V}$ , however, the deviation shows at higher  $V_{gs}$ , which is due to the aforementioned mobility degradation. In addition, the contact-limited conduction in the OTFT may also affect the current and the mobility, which needs further verification. Note that, for the simulated curves of device B that eliminates mobility degradation, the ON-current is approximately one order of magnitude higher than the one of device A, indicating

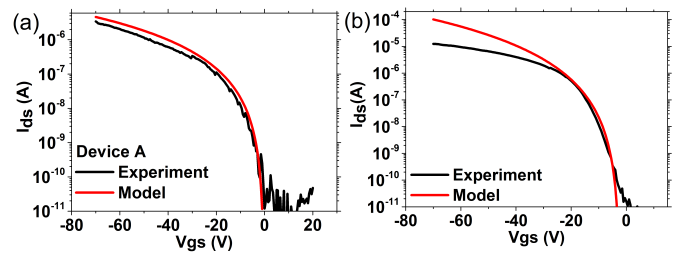


Fig. 4. Modeling of (a) device A and (b) device B based on hopping transport mechanism.

the effect of higher mobility enhancement factor of device B that is related to the lower energy/space disorder of the active layer.

Note that, for our case, the flat-band voltage is adopted to deduce the mobility enhancement factor and simulate the transfer curves, which is consistent with [9] that adopts Gauss's law. Indeed, the deep states are calculated from flat-band voltage, and are used for the verification of mobility enhancement factor. The tail distribution traps theory [13], [14] may also work, which needs further verification. In addition, the band conduction transport can be negligible due to the positive mobility enhancement factor.

The microscopic energy/space disorder of active layer may be related with macroscopic morphology of active layer. In the hopping transport, the disorder in energy/space is due to that for organic semiconductors, the structural disorder of amorphous or small polycrystalline morphology makes the conventional transport energy band split into random-spacing, energy-disordered localized states, which can localize the carriers and form hopping sites. For smaller disorder with less hopping sites, DOS decreases, which reflects a larger mobility enhancement factor in (9) as when DOS is smaller, the characteristic temperature  $T_0$  is larger in (4) of the exponential DOS.

Atomic force microscopy (AFM) observations of the pentacene active layer were carried out for devices A and B. From Fig. 5(a) and (b), for both devices A and B, the morphologies of active layer were dendritic shapes with high crystalline quality, however, for device A with smaller mobility enhancement factor, abundant microcrystals appear. The microcrystals formation may be due to the relatively low vacuum degree of approximately  $2 \times 10^{-4} \text{ Pa}$ , which helps to form island-like grains. The detailed influencing factors should be further investigated. Nevertheless, the energy/space disorder in the active layer of device A is more severe than device B, as indicated from roughness images of Fig. 5(c) and (d). As mentioned above, the energy/space disorder affects the mobility enhancement factor and thus the electrical characteristics. For the active layer AFM morphologies, the better morphology with larger crystallinity corresponds to smaller density of localized states, and therefore results in larger field effect mobility. Indeed, even though the relationship between the morphology and the DOS/mobility enhancement factor can be qualitatively illustrated, the quantitative relation is hard to be given. Nevertheless, the VRH mechanism may still be consistently verified.

Finally, in Table II, the electrical characteristics in this work are compared with the previously reported publications based

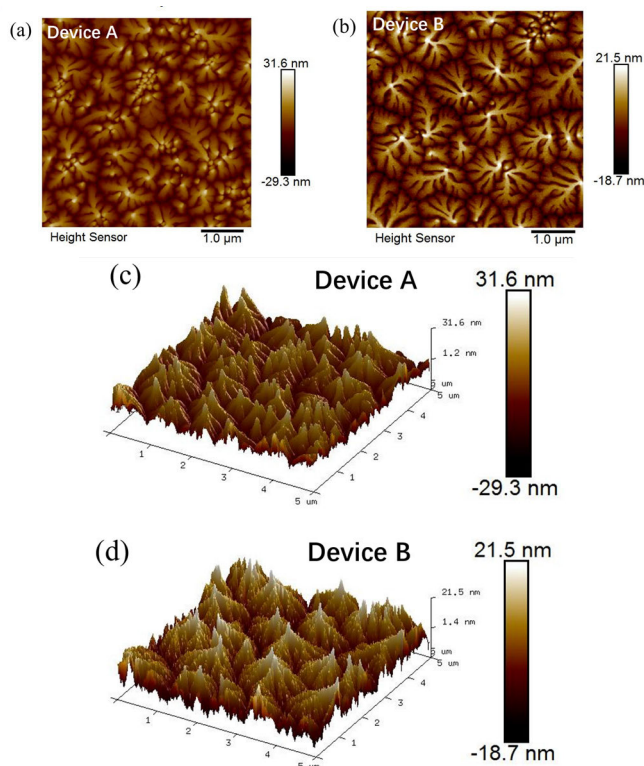


Fig. 5. AFM morphology of active layer in (a) device A and (b) device B. Roughness image of active layer in (c) device A and (d) device B.

on polymer gate dielectrics. From the comparison,  $I_{ON}/I_{OFF}$  ratio of approximately  $3.6 \times 10^5$  and threshold voltage of about  $-16.8$  V is moderate, and the effective mobility of  $1.62$   $\text{cm}^2/\text{V}\cdot\text{s}$  is superior to reported values. In fact, the high effective mobility is achieved even with mobility degradation, which shows the advantage of high mobility using this simple PS decoration method. Further work can be on the improvement of effective mobility without mobility degradation.

#### IV. CONCLUSION

Bottom-gate, top-contact OTFTs with pentacene active layers were fabricated and analyzed. The electrical parameters were deduced, with approximately same threshold voltage of  $-16$  V for both devices A and B, and smaller subthreshold slope of device B. The mobility enhancement factor is smaller for device A, which is related to the characteristic temperature of exponential DOS. By adopting current model of hopping transport mechanism, the experimental data fit the modeled current well. The morphologies of organic semiconductor active layers were observed, the dendritic microcrystals of device A show higher energy/space disorder, which is consistent with the low mobility enhancement factor of device A, and thus degrades the electrical characteristics. The electrical characteristics of this work were comparable to previously reported publications.

#### REFERENCES

- [1] S. Nam et al., "Poly(2-alkyl-2-oxazoline) electrode interlayers for improved n-type organic field effect transistor performance," *Appl. Phys. Lett.*, vol. 115, Sep. 2019, Art. no. 143302, doi: <https://doi.org/10.1063/1.5118337>.
- [2] R. Sarma and D. Saikia, "Low-cost  $\text{MoO}_3/\text{Al}$  bilayer electrode for pentacene-based OTFTs," *IEEE Electron Device Lett.*, vol. 32, no. 2, pp. 209–211, Feb. 2011, doi: [10.1109/LED.2010.2093502](https://doi.org/10.1109/LED.2010.2093502).
- [3] C. Y. Han, Y. X. Ma, W. M. Tang, X. L. Wang, and P. T. Lai, "A study on pentacene organic thin-film transistor with different gate materials on various substrates," *IEEE Electron Device Lett.*, vol. 38, no. 6, pp. 744–747, Jun. 2017, doi: [10.1109/LED.2017.2695538](https://doi.org/10.1109/LED.2017.2695538).
- [4] A. Tewari et al., "High-mobility and low-operating voltage organic thin film transistor with epoxy based siloxane binder as the gate dielectric," *Appl. Phys. Lett.*, vol. 107, Sep. 2015, Art. no. 103302, doi: <https://doi.org/10.1063/1.4930305>.
- [5] O. D. Jurchescu, M. Popinciuc, B. J. van Wees, and T. T. M. Palstra, "Interface-controlled, high-mobility organic transistors," *Adv. Mater.*, vol. 19, no. 5, pp. 688–692, Mar. 2007, doi: [10.1002/adma.200600929](https://doi.org/10.1002/adma.200600929).
- [6] H. Fukagawa et al., "High-current operation of vertical-type organic transistor with preferentially oriented molecular film," *AIP Adv.*, vol. 6, no. 4, Apr. 2016, Art. no. 045010, doi: [10.1063/1.4947203](https://doi.org/10.1063/1.4947203).
- [7] O. Marinov, M. J. Deen, C. Feng, and Y. Wu, "Precise parameter extraction technique for organic thin-film transistors operating in the linear regime," *J. Appl. Phys.*, vol. 115, no. 3, Jan. 2014, Art. no. 034506, doi: [10.1063/1.4862043](https://doi.org/10.1063/1.4862043).
- [8] M. C. J. M. Vissenberg and M. Matters, "Theory of the field-effect mobility in amorphous organic transistors," *Phys. Rev. B, Condens. Matter*, vol. 57, no. 20, pp. 12964–12967, May 1998, doi: [10.1103/PhysRevB.57.12964](https://doi.org/10.1103/PhysRevB.57.12964).
- [9] T. Suzuki, Y. Osaka, and M. Hirose, "Theoretical interpretations of the gap state density determined from the field effect and capacitance-voltage characteristics of amorphous semiconductors," *Jpn. J. Appl. Phys.*, vol. 21, no. 3A, p. L159, Mar. 1982, doi: [10.1143/JJAP.21.L159](https://doi.org/10.1143/JJAP.21.L159).
- [10] M. J. Deen, O. Marinov, U. Zschieschang, and H. Klauk, "Organic thin-film transistors: Part II—Parameter extraction," *IEEE Trans. Electron Devices*, vol. 56, no. 12, pp. 2962–2968, Dec. 2009, doi: [10.1109/TED.2009.2033309](https://doi.org/10.1109/TED.2009.2033309).
- [11] W. L. Kalb, K. Mattenberger, and B. Batlogg, "Oxygen-related traps in pentacene thin films: Energetic position and implications for transistor performance," *Phys. Rev. B, Condens. Matter*, vol. 78, Jul. 2008, Art. no. 035334, doi: [10.1103/PhysRevB.78.035334](https://doi.org/10.1103/PhysRevB.78.035334).
- [12] E. Calveti, L. Colalongo, and Z. M. Kovács-Vajna, "Organic thin film transistors: A DC/dynamic analytical model," *Solid-State Electron.*, vol. 49, no. 4, pp. 567–577, Apr. 2005, doi: [10.1016/j.sse.2005.01.006](https://doi.org/10.1016/j.sse.2005.01.006).
- [13] O. Marinov, M. J. Deen, and R. Datar, "Compact modeling of charge carrier mobility in organic thin-film transistors," *J. Appl. Phys.*, vol. 106, no. 6, Sep. 2009, Art. no. 064501, doi: [10.1063/1.3212539](https://doi.org/10.1063/1.3212539).
- [14] P. Servati, A. Nathan, and G. A. J. Amaratunga, "Generalized transport-band field-effect mobility in disordered organic and inorganic semiconductors," *Phys. Rev. B, Condens. Matter*, vol. 74, no. 24, p. 245210, Dec. 2006, doi: [10.1103/PhysRevB.74.245210](https://doi.org/10.1103/PhysRevB.74.245210).
- [15] G. Abbas, Z. Ding, K. Mallik, H. Assender, and D. M. Taylor, "Hysteresis-free vacuum-processed acrylate-pentacene thin-film transistors," *IEEE Electron Device Lett.*, vol. 34, no. 2, pp. 268–270, Feb. 2013, doi: [10.1109/LED.2012.2234434](https://doi.org/10.1109/LED.2012.2234434).
- [16] H. Moon, M. Kim, and S. Yoo, "Bilayer source/drain electrodes self-aligned with fluoropolymer dielectrics for stable high-performance organic TFTs," *IEEE Electron Device Lett.*, vol. 32, no. 8, pp. 1137–1139, Aug. 2011, doi: [10.1109/LED.2011.2157800](https://doi.org/10.1109/LED.2011.2157800).
- [17] M. Petrosino, A. Rubino, R. Miscioscia, A. De Girolamo Del Mauro, and C. Minarini, "Effects of the polymeric dielectric on OTFT performances," in *Proc. 3rd Int. Conf. Signals, Circuits Syst. (SCS)*, Medenine, Tunisia, Nov. 2009, Art. no. 11150591, doi: [10.1109/ICSCS.2009.5412549](https://doi.org/10.1109/ICSCS.2009.5412549).
- [18] J. Jakabovic, J. Kovac, R. Smajnek, J. Kovac, M. Sokolsky, and D. Hasko, "Pentacene OTFT with parylene gate dielectric," in *Proc. Int. Conf. Adv. Semiconductor Devices Microsystems*, Smolenice Castle, Slovakia, 2008, p. 147, doi: <https://doi.org/10.1109/ASDAM.2008.4743302>.
- [19] S. Zhou, M. Li, Q. Tang, Z. Song, Y. Tong, and Y. Liu, "Deposition of pentacene thin film on polydimethylsiloxane elastic dielectric layer for flexible thin-film transistors," *IEEE Electron Device Lett.*, vol. 38, no. 8, pp. 1031–1034, Aug. 2017, doi: [10.1109/LED.2017.2714845](https://doi.org/10.1109/LED.2017.2714845).
- [20] Y. Jang et al., "Surface treatments of poly(4-vinyl phenol) insulator for high-performance pentacene thin-film transistors," *IEEE Trans. Device Mater. Rel.*, vol. 17, no. 3, pp. 522–525, Sep. 2017, doi: [10.1109/TDMR.2017.2716962](https://doi.org/10.1109/TDMR.2017.2716962).